Transport in Porous Media **23:** 275–301, 1994.

The Influence of Free Convection on Soil Salinization in Arid Regions

ARKADY GILMAN
Dept. of Geological Sciences, University of British Columbia, 6339 Stores Rd., Vancouver, B.C., Canada V6T 1Z4

JACOB BEAR
Faculty of Civil Engineering, Technion – Israel Institute of Technology, Haifa, 32000, Israel

Received: 14 March 1995; in final form: 20 December 1995)

Abstract. Evaporation of groundwater in a region with a shallow water table and small natural replenishment causes accumulation of salts near the ground surface. Water in the upper soil layer becomes denser than in the depth. This is a potentially unstable situation which may result in convective currents. When free convection takes place, estimates of the salinity profile, salt precipitation rate, etc., obtained within the framework of a 1-D (vertical) model fail.

Very simplified model of the process is proposed, in which the unsaturated zone is represented by a horizontal soil layer at a *constant* water saturation, and temperature changes are neglected. The purpose of the model is to obtain a rough estimate of the role of natural convection in the salinization process.

A linear stability analysis of a uniform vertical flow is given, and the stability limit is determined numerically as a function of evaporation rate, salt concentration in groundwater, and porous medium dispersivity. The loss of stability corresponds to quite realistic Rayleigh numbers. The stability limit depends in nonmonotonic way on the evaporation rate.

The developed convective regime was simulated numerically for a 2-D vertical domain, using finite volume element discretization and FAS multigrid solver. The dependence of the average salt concentration in the upper layer on the Rayleigh number was obtained.

Key words: free convection, through flow, vadoze zone, salinization, dispersion, multigrid

1. List of Main Symbols

a	horizontal wavenumber
a_L, a_T	dispersivities (longitudinal and transversal)
$\mathcal{D}^*$	diffusion coefficient (in a porous medium)
g	acceleration of gravity
H	thickness of the vadoze zone
k	permeability
p	pressure
Pe	Péclet number
q	mass flux
Ra	Rayleigh number

Greek

α_L, α_T	dimensionless dispersivities
β	coefficient of concentration expansion
γ	coefficient of viscosity variation
θ	volumetric fraction of the liquid phase
μ	viscosity
ρ	density
ψ	stream function
ω	mass fraction of salt in water

Vectors and tensors

D	dispersion coefficient
e	unit vector
I	unit tensor
J	nonadvective salt flux
V	liquid phase velocity
x	radius-vector

2. Introduction

Evaporation of soil moisture from ground surface is one of the main mechanisms that cause soil salinization. It plays a major role when the water table is present at a relatively shallow depth, and the natural replenishment is very small, as in arid regions. Under such conditions, the average flow of water through the unsaturated soil is directed upwards. If groundwater is saline (and to some extent it usually is), this flow transports salts towards ground surface. Water evaporates from the upper soil layer, while salts remain in the soil and their concentration increases.

Usually, such processes (i.e., rainfall infiltration, drying, etc.) are analyzed by using a 1-D (vertical) model, assuming that the flow is uniform (cf. Bresler *et al.* [4], Hillel [6]). To some extent, the aim of the present work is to check the robustness of the 1-D approach in the simplest steady or quasi-steady flow regimes.

If the boundary conditions at ground surface and at the water table do not change, sooner or later, the system will come to a steady state. If the vertical uniform flow is assumed, then the liquid mass flux, q, and the salt mass flux, q^s, are constant, while the salt concentration depends only on the vertical coordinate. The total mass flux of salt in the soil is made up of an advective flux and a diffusive-dispersive one:

$$q^s = q\omega - \theta\rho D_h \frac{\mathrm{d}\omega}{\mathrm{d}z}, \tag{1}$$

where ρ is the density of the liquid phase, ω is the mass fraction of salt in it, $D_h = D_h(q, \theta)$ is the coefficient of hydrodynamic dispersion of salt in the porous medium, $\theta(z)$ is the volumetric fraction of the liquid phase, and z is vertical coordinate (positive upwards, with the origin at the water table). We may assume

that salt concentration at the water table, $z = 0$, is equal to the average groundwater salinity, ω_0:

$$z = 0 : \quad \omega = \omega_0. \tag{2}$$

There is no salt transport through ground surface, at $z = H$. If the salt concentration is below the maximal solubility of salt in water, then the condition at this boundary is that of no-flux:

$$z = H : \quad q^s = 0, \quad (\omega < \omega_*), \tag{3}$$

where ω_* denotes the mass fraction of salt in saturated brine. If the salt concentration at ground surface reaches the maximal solubility threshold, we have a Dirichlet boundary condition:

$$z = H : \quad \omega = \omega_*. \tag{4}$$

Then the upward salt flux can be positive, the excess salt precipitating just below the ground surface.

From the single first-order ordinary differential equation (1), with the two boundary conditions (2) and (3)–(4), the unknown salt flux, q^s, and the distribution of dissolved salt, $\omega(z)$, can be determined, if we assume $\theta(z)$ to be known. In the case without salt precipitation, we obtain from (1)–(3):

$$\ln\frac{\omega_1}{\omega_0} = q\int_0^H \frac{\mathrm{d}z}{\theta\rho D_h} = \frac{qH}{\overline{\theta}\overline{\rho}\overline{D}_h} = \frac{\overline{V}H}{\overline{D}_h}, \tag{5}$$

where ω_1 is the mass fraction of salt in the solution near ground surface, $V = q/(\theta\rho)$ is the liquid velocity, and a bar over a variable denotes its value at some internal point of the layer. The expression on the right-hand side of (5) is the Péclet number, Pe, of the problem. From (5) and (3) we can see that under steady-state precipitation takes place as long as the Péclet number exceeds its critical value, Pe*

$$\mathrm{Pe} > \mathrm{Pe}^* \equiv \ln\frac{\omega_*}{\omega_0}.$$

Typical salt concentrations in groundwater are in the range $10^2\mathrm{mg/l} \div 10^4\mathrm{mg/l}$ (i.e., $10^{-4} < \omega < 10^{-2}$). Under normal conditions, the maximum solubility of, say, NaCl in water is about 310g/l ($\omega \simeq 0.26$). Thus, the critical Péclet number is in the range $3 < \mathrm{Pe}^* < 8$. On the other hand, let us estimate the actual Péclet number for a capillary rise caused by evaporation from ground surface. Taking $\overline{V} = 10^{-7}\mathrm{m/s} \simeq 8\mathrm{mm/day}$ (typical evaporation rate for dry and hot regions), $\overline{D}_h = 10^{-9} \div 10^{-8}\mathrm{m^2/s}$, $H = 0.5 \div 3\mathrm{m}$, we obtain Pe in the range 5 to 300.

This means that in most cases $\mathrm{Pe} > \mathrm{Pe}^*$. Therefore, one may conclude that a shallow water table without natural or artificial leaching necessarily implies soil salinization. For example, this pessimistic conclusion leaves no chance for oases in deserts to exist.

Actually, there is a danger of overestimating the rate of salt accumulation inherent in the assumption of a one-dimensional flow pattern. According to the distribution described by (5), water near ground surface is more saline and, hence, denser than that at larger depths. This is a potentially unstable situation which may result in convective currents. If such currents arise, they provide a much better 'mixing' mechanism for salt in the unsaturated zone than that due to molecular diffusion and mechanical dispersion. Under certain conditions, salinization may be prevented.

It is hardly worth attacking this problem by writing a detailed mathematical model which takes into account all the relevant physical phenomena and then solve it by a straightforward numerical simulation. As far as free convection is concerned, the set of differential equations to be solved will, probably, have more than one solution (and even more than one *stable* solution). An ordinary simulator, at best, will give us an approximation of one of these solutions without even informing us that it is not unique. As in many other cases of computer experiments, one should have a good (at least, qualitative) estimate of the result *before* turning to the detailed numerical simulation runs. For this reason, it is necessary to start from some simplified model which can be investigated by analytical or semi-analytical methods, yielding guidelines for future numerical simulation.

Free convection in unsaturated porous media is a subject that has hardly been investigated. With this observation in mind, in the current work we shall model the unsaturated zone as a porous medium layer with a *uniform* moisture distribution, and assume that the latter is not influenced by the flow. Under these assumptions, the problem becomes similar to that for a saturated porous medium, except that we have to use values of permeability, diffusion coefficient, and dispersivity that correspond to the assumed saturation. We may then vary the saturation within the framework of a sensitivity analysis.

A closely related problem of thermally induced natural convection with vertical through flow was studied for the first time by Wooding [16]. He investigated analytically the stability of a thermal boundary layer arising when hot water in an infinitely deep geothermal reservoir flows upwards through a permeable horizontal surface where it is cooled. He found that this one-dimensional flow is linearly unstable if the modified Darcy–Rayleigh number, Ra' (the modification is needed to take into account viscosity dependence on temperature), exceeds some critical value, Ra^*, which is proportional to the flow velocity.

Homsy and Sherwood [7] expanded Wooding's analysis to the case of a finite layer of saturated porous medium heated from below, through which liquid is ejected at a constant rate. When the through flow is zero, this problem is reduced to the well investigated porous-medium analog of the Rayleigh–Bénard problem. When the thermal Péclet number is large, only the boundary layer is of interest, and the problem becomes very similar to that studied by Wooding. Homsy and Sherwood obtained (numerically) the dependence of the critical Rayleigh number on Pe in the linear (Ra_L^*) and energy (Ra_E^*) limits, i.e., they found sufficient

conditions for unconditional stability and for instability to small perturbations. Both functions of Pe are monotonic, have a common limit ($= 4\pi^2$) at Pe $= 0$, and increase approximately linearly as Pe $\to \infty$. Contrary to the case of Pe $= 0$, in general, $\mathrm{Ra}_E^*(\mathrm{Pe})$ is significantly less than $\mathrm{Ra}_L^*(\mathrm{Pe})$, i.e., there exists a certain range of parameters for which the basic one-dimensional flow is stable with respect to small perturbations, but other flow regimes may also exist. Linear stability limits for some other types of boundary conditions were calculated by Jones and Persichetti [8]. The qualitative behavior of $\mathrm{Ra}_L^*(\mathrm{Pe})$ curves was shown to be similar for various boundary conditions, but quantitatively, the ranges of stability were found to differ strongly.

The problem we consider here differs in several ways from those reviewed above. The major factor influencing stability is salinity rather than temperature variations and the latter will be neglected in our model. The through flow in the problem at hand is not just a superposed stabilizing factor; in fact, it is the only factor causing instability. This results in a nonmonotone dependence of the stability limit on the through flow rate (expressed by the Péclet number). We also take into account mechanical dispersion, which may be neglected when studying stability of a stagnant state, but is a significant factor when through flow is involved. Finally, in our case the concentration drop between the bottom and the top of the layer is not small (although their ratio is small) and this does not permit us to neglect viscosity variations.

3. Mathematical Model

3.1. BASIC ASSUMPTIONS

Let us consider a horizontal infinitely long porous medium layer of thickness H. We shall assume that

A1. The porous matrix is rigid, chemically inert, isotropic and homogeneous.
A2. The void space contains a uniformly distributed, two-component (water and salt) liquid.
A3. Liquid flow is so slow that inertial effects in the momentum balance equation may be neglected and Darcy's law is applicable.
A4. The system is under isothermal conditions.
A5. Fick's law describes diffusion and Fickian type law describes dispersion. The diffusion coefficient and dispersivity are independent of salt concentration.
A6. The density and dynamic viscosity of the liquid depend linearly on salt concentration.
A7. The influence of density variations may be neglected in all terms except for the one expressing the gravity force.

In reality, seasonal temperature variations may influence the process. Heating of the upper soil layer during the hot seasons reduces the liquid density and, hence, has some stabilizing effect opposite to that of salt concentration. The relative

importance of these two factors (temperature and composition) for the stability of the motion can be estimated from the ratio of the corresponding Rayleigh numbers, Ra_T (thermal) and Ra_C (concentrational):

$$\frac{\mathrm{Ra}_T}{\mathrm{Ra}_C} = \frac{(\Delta\rho)_T}{D_T} \Big/ \frac{(\Delta\rho)_C}{D_h} = \frac{D_h \theta C_f}{\lambda_{\mathrm{pm}}} \frac{(\Delta\rho)_T}{(\Delta\rho)_C}, \tag{6}$$

where $D_T \equiv \lambda_{\mathrm{pm}}/(\theta C_f)$ is the thermal diffusivity of the (unsaturated) porous medium, λ_{pm} is its thermal conductivity, C_f is the volumetric heat capacity of the liquid, and $(\Delta\rho)_T$ and $(\Delta\rho)_C$ are the characteristic density variations due to heating and compositional change, respectively. To obtain an estimate, let us assume $D_h = 10^{-4}\mathrm{cm}^2/\mathrm{s}$ (it is 3 times *greater* than molecular diffusion in bulk water and corresponds to the dispersivity $a_L = 10\mathrm{cm}$ and velocity $V \simeq 10\mathrm{mm/day}$), $\theta = 0.2$, $C_f = 1\mathrm{cal}/^\circ\mathrm{C}\,\mathrm{cm}^3$, $\lambda_{\mathrm{pm}} = 2.10^{-3}\mathrm{cal/cm \cdot s \cdot {}^\circ C}$ (wet sand or clay). The density variation due to the change of temperature from 40°C to 10°C is $(\Delta\rho)_T = 7.5\mathrm{kg/m}^3$, while the difference of densities of 10% NaCl solution and of pure water is $(\Delta\rho)_C = 75\mathrm{kg/m}^3$. Substituting these values into (6), we arrive at

$$\frac{\mathrm{Ra}_T}{\mathrm{Ra}_C} = 10^{-3}.$$

For this reason, we do not take temperature changes into account in A4. Note, however, that a nonuniform temperature distribution has an indirect effect on the processes under consideration, due to vapor diffusion from hot to cool regions (see Bear and Gilman [2]).

The statement A7 is usually referred to as the *Overberk–Boussinesq assumption* (see Joseph [9]). Long practice has shown that it provides qualitatively correct results. On the other hand, the viscosity dependence on concentration is significantly greater than that of the density (viscosity of a brine is usually 1.5–3 times higher than that of pure water, while the density variations do not exceed 15–30%). This explains why we do take viscosity changes into account, though it also does not influence the results qualitatively.

Some additional assumptions will be introduced later on.

3.2. MODEL EQUATIONS AND BOUNDARY CONDITIONS

Under the above assumptions, the motion in the considered porous medium domain is described by a set of two mass balance equations (for the liquid as a whole and for salt component), a momentum balance equation for the liquid, that takes the form of Darcy's law, and constitutive relations for nonadvective salt flux, density and viscosity of the liquid. These equations are

$$\nabla \cdot \boldsymbol{V} = 0, \tag{7}$$

$$\partial_t \omega = -\nabla \cdot (\boldsymbol{V}\omega + \boldsymbol{J}), \tag{8}$$

$$\theta \boldsymbol{V} = -\frac{k}{\mu}(\nabla p + \rho g \nabla z), \tag{9}$$

$$\boldsymbol{J} = -\mathbf{D}_h \nabla\omega, \tag{10}$$

$$\rho = \rho_0(1+\beta\omega), \quad \mu = \mu_0(1+\gamma\omega). \tag{11}$$

Here, $k = k(\theta)$ is the liquid phase permeability, $\boldsymbol{J}$ is the volumetric nonadvective salt flux, μ is the liquid viscosity, β is the coefficient of concentration expansion, and γ is the coefficient of viscosity variation. The nonadvective salt flux is due to molecular diffusion and mechanical dispersion. Taking assumption A1 into account, and following common practice (see Bear and Bachmat [1]), we assume that the coefficient of mechanical dispersion, $\mathbf{D}$, is expressed by symmetric second rank tensor, proportional to V, for which $\boldsymbol{V}$ is the maximal eigenvector:

$$\mathbf{D}_h = \mathcal{D}^*\mathbf{I} + \mathbf{D},$$

$$\mathbf{D} = a_T V\mathbf{I} + (a_L - a_T)\sum_{i,j}\frac{V_i V_j}{V}\,\mathbf{e}_i\otimes\mathbf{e}_j \quad (i,j\in\{x,y,z\}). \tag{12}$$

Here $\mathcal{D}^* = \mathcal{D}^*(\theta)$ is the diffusion coefficient of salt in liquid in a porous medium, a_L and a_T are, respectively, longitudinal and transversal dispersivities, $\mathbf{e}_x$, $\mathbf{e}_y$, $\mathbf{e}_z$ are unit vectors of the Cartesian coordinate system (x, y, z), $\mathbf{I}$ is the unit tensor, V_i are the components of the velocity vector $\boldsymbol{V}$, and V is its magnitude.

For each of the two mass balance equations, we need boundary conditions at the top and the bottom of the layer. As far as the water table constitutes the bottom boundary, the pressure on this boundary is constant (and we may choose it to be zero). We shall also assume, that good mixing takes place within the aquifer, such that the concentration of salt there is constant and equal to ω_0. Thus, we have the condition:

$$z = 0: \quad p = 0, \quad \omega = \omega_0 = \text{const}. \tag{13}$$

The boundary condition for salt at ground surface should express the fact that salt cannot leave the layer through it. However, there is an additional constraint: $\omega \le \omega_*$ where ω_* is the maximum solubility of salt in water. If, in some part of the boundary, the concentration reaches ω_*, and the net salt flux is directed towards the boundary, the excess salt will precipitate there. We shall assume that the precipitation takes place just at the boundary, and that the precipitate does not change either the evaporation rate or the porosity and permeability of the porous medium. In the general case, two kinds of boundary condition for salt may occur at ground surface: along part of the boundary (let us denote it $\mathcal{B}_1$) the salt flux is zero, while on the other ($\mathcal{B}_2$) the concentration of salt is equal to ω_*:

$$z = H: \quad \begin{cases} \text{on } \mathcal{B}_1: & V_z\omega + J_z = 0,\ \omega \le \omega_*, \\ \text{on } \mathcal{B}_2: & \omega = \omega_*, \qquad V_z\omega + J_z \ge 0. \end{cases} \tag{14}$$

This condition is nonlinear, because the decomposition of the boundary is not known a-priori and should be determined as part of the solution.

The problem of proper boundary conditions for liquid flow at ground surface, taking evaporation into account, has been widely discussed in the literature (e.g., Monteith [11]). For the sake of simplicity, we shall assume that evaporation rate at the top of our domain is a given constant, E. Let V_0 denote the liquid velocity as if it were pure water, $V_0 = E/\rho_0\theta$. Though the total mass flux of liquid phase on $\mathcal{B}_2$ is greater than that of water component, the difference, i.e., the salt flux, is relatively small (its contribution is of the order of ω_0/ω_*). Thus, we shall assume that the boundary condition

$$z = H : \quad V_z = V_0 \tag{15}$$

holds on the entire ground surface.

Let us introduce dimensionless quantities

$$\hat{\mathbf{x}} = H^{-1}\mathbf{x}, \quad \hat{t} = \frac{\mathcal{D}^*}{H^2}t, \quad \hat{\boldsymbol{V}} = \frac{H}{\mathcal{D}^*}\boldsymbol{V},$$

$$\hat{\boldsymbol{J}} = \frac{H}{\mathcal{D}^*}\boldsymbol{J}, \quad \hat{p} = \frac{k}{\mu_0\theta\mathcal{D}^*}(p + \rho_0 g z).$$

The dimensionless forms of (7)–(11) are

$$\hat{\nabla}\cdot\hat{\boldsymbol{V}} = 0, \tag{16}$$

$$\partial_{\hat{t}}\omega = -\hat{\nabla}\cdot(\hat{\boldsymbol{V}}\omega + \hat{\boldsymbol{J}}), \tag{17}$$

$$(1+\gamma\omega)\hat{\boldsymbol{V}} = -\hat{\nabla}\hat{p} - \mathrm{Ra}\omega\hat{\nabla}\hat{z}, \tag{18}$$

$$\begin{aligned}\hat{\boldsymbol{J}} &= -\hat{\mathbf{D}}_h\cdot\hat{\nabla}\omega \\ &= -\left[(1+\alpha_T\hat{V})\mathbf{I} + (\alpha_L - \alpha_T)\sum_{i,j}\frac{\hat{V}_i\hat{V}_j}{\hat{V}}\mathbf{e}_i\otimes\mathbf{e}_j\right]\cdot\hat{\nabla}\omega,\end{aligned} \tag{19}$$

where $\alpha_L = a_L/H$ and $\alpha_T = a_T/H$ are dimensionless dispersivities, and

$$\mathrm{Ra} = \frac{k\rho_0\beta g H}{\mu_0\theta\mathcal{D}^*} \tag{20}$$

is the concentrational Darcy–Rayleigh number for the problem under consideration. Note that Rayleigh number is usually defined to include the drop in concentration, $\omega_1 - \omega_0$, between the top and the bottom of the domain. In our case, this concentration difference is not prescribed and can only be determined from the solution. Even in a steady state, the concentration at the top, $\omega_1 \leq \omega_*$, may vary along ground surface.

Boundary conditions (13)–(15) transform to the following dimensionless form:

$$\hat{z} = 0 : \quad \hat{p} = 0, \quad \omega = \omega_0, \tag{21}$$

$$\hat{z} = 1 : \quad \hat{V}_z = \mathrm{Pe}, \quad \begin{cases} \text{on } \mathcal{B}_1 : & \mathrm{Pe}\,\omega + \hat{J}_z = 0 \ (\omega \le \omega_*) \\ \text{on } \mathcal{B}_2 : & \omega = \omega_* \qquad (\mathrm{Pe}\omega + \hat{J}_z \ge 0). \end{cases} \tag{22}$$

Here, the Péclet number is defined according to the vertical component of the liquid velocity at ground surface, $\mathrm{Pe} = V_0 H/\mathcal{D}^*$. In what follows we shall work only in dimensionless variables, omitting the hat accents.

3.3. ONE-DIMENSIONAL SOLUTIONS

The one-dimensional steady state solution may be obtained from (16)–(22), by substituting

$$\partial_t \omega = 0, \quad V_x = V_y = 0, \quad V_z = \mathrm{Pe}, \quad \omega = \omega(z).$$

From (19), it can easily be found that

$$J_z = -(1 + \alpha_L \mathrm{Pe})\frac{\mathrm{d}\omega}{\mathrm{d}z},$$

and, hence, $\omega(z)$ satisfies

$$\mathrm{Pe}\omega - (1 + \alpha_L \mathrm{Pe})\frac{\mathrm{d}\omega}{\mathrm{d}z} = \text{const}, \quad \omega(0) = \omega_0. \tag{23}$$

While $\omega_1 < \omega_*$, the constant is equal to zero, and

$$\omega(z) = \omega_0 \mathrm{e}^{\mathrm{Pe}' z}, \tag{24}$$

where

$$\mathrm{Pe}' = \frac{\mathrm{Pe}}{1 + \alpha_L \mathrm{Pe}} \tag{25}$$

is the modified Péclet number which uses the longitudinal coefficient of hydrodynamic dispersion as a reference, instead of the molecular diffusion. Note that while Pe may take any positive value, Pe′ is always less than α_L^{-1}. The critical value of Pe′, corresponding to the onset of precipitation, is

$$\mathrm{Pe}^* = \ln \frac{\omega_*}{\omega_0}.$$

When $\mathrm{Pe}^* > \mathrm{Pe}^*$, the constant in (23) is unknown, but $\omega(1) = \omega_*$. The solution has the form

$$\omega(z) = \omega_0 + (\omega_* - \omega_0)\frac{e^{\mathrm{Pe}' z} - 1}{\mathrm{e}^{\mathrm{Pe}'} - 1}, \quad (\mathrm{Pe}' \ge \mathrm{Pe}^*). \tag{26}$$

For the rest of the study, we shall assume that $\omega_0 \ll \omega_*$. Then (26), up to $O(\omega_0/\omega_*)$, is equivalent to

$$\omega(z) = \omega_* e^{Pe'(z-1)}. \tag{27}$$

For $Pe' > Pe^*$ the distribution $\omega(z, t_*)$, corresponding to the moment, t_*, of the onset of precipitation, is also of interest, as it proves to be the 'most unstable' transient state (see the next section). Although for special initial conditions (e.g., for $\omega(z, 0) \equiv \omega_0$), the solution of the unsteady 1-D problem can be found in a closed analytical form, for our purpose a simple rough approximation of $\omega(z, t_*)$ will suffice. Let us only assume that for $t \geq t_*$ $\partial_t \omega \geq 0$ for all z (i.e., that the system has already 'forgotten' its initial conditions). Then, with

$$u = \omega(z, t_*) - \omega_* e^{Pe'}(z - 1)$$

we have

$$\begin{aligned} &\frac{d^2u}{dz^2} - Pe'\frac{d^2u}{dz^2} \geq 0, \quad 0 < z < 1, \\ &z = 1 : \quad u = 0, \quad \frac{d^2u}{dz^2} - Pe'u = 0. \end{aligned} \tag{28}$$

From this differential inequality it follows that $u \geq 0$ for $0 < z < 1$, and, hence,

$$\omega(z, t_*) \geq \omega_* e^{Pe'(z-1)}.$$

On the other hand, as long as $\partial_t \omega \geq 0$, $\omega(z, t_*)$ at any point is less than the final ($t \to \infty$) concentration at that point. Comparing with (27), we conclude that the latter gives also the approximation of $\omega(z, t_*)$ up to $O(\omega_0/\omega_*)$. Note that the concentration profile given by (27) is independent of the boundary condition at the bottom of the region, i.e., the solution has the nature of a boundary layer.

4. Linear Stability Analysis of the Upward Flow

Let $\tilde{p}(z)$, $\tilde{V}(z) \equiv Pe\mathbf{e}_z$, and $\tilde{\omega}(z)$ be a one-dimensional steady-state solution of (16)–(22), which we shall refer to as *basic solution*. We wish to find sufficient conditions for the onset of free convection, i.e., for the *instability* of the basic solution. These sufficient conditions may be found by studying the fate of small perturbations of the basic solution. In the same way, we may analyze stability of a transient quasi steady state (see Nield [12]).

In this section we shall refer to the three basic solutions:

C1. Steady-state solution for small Péclet numbers ($Pe' < Pe^*$) given by (24).
C2. Steady-state solution for large Péclet numbers ($Pe' > Pe^*$).
C3. Transient state just before the onset of precipitation ($Pe' > Pe^*$).

In the cases C2 and C3, we shall use the same approximate formula (27) for the concentration profile. However, after the onset of precipitation (case C2), the concentration satisfies Dirichlet boundary condition at the top boundary (i.e., the entire boundary is of $\mathcal{B}_2$ type), while prior to the onset of precipitation it satisfies a no-flow condition (cf. (14)). We shall see that this difference has an effect on the class of the small perturbations allowed and, hence, on the stability conditions.

4.1. EIGENPROBLEM FORMULATION

Let us introduce

$$p = \tilde{p} + \mathring{p}, \quad \boldsymbol{V} = \mathrm{Pe}\mathbf{e}_z + \mathring{\boldsymbol{V}}, \quad \omega = \tilde{\omega} + \mathring{\omega}, \tag{29}$$

where $\mathring{p}$, $\mathring{\boldsymbol{V}} = \sum \mathring{V}_i \mathbf{e}_i$, and $\mathring{\omega}$ are small perturbations. The magnitude of the perturbed velocity vector is

$$\left|\tilde{\boldsymbol{V}} + \mathring{\boldsymbol{V}}\right| = \mathrm{Pe} + \mathring{V}_z + \mathrm{O}(\mathring{V}^2).$$

The perturbation of the tensor

$$\mathbf{T}(\boldsymbol{V}) \equiv \sum_{i,j} \frac{V_i V_j}{V} \mathbf{e}_i \otimes \mathbf{e}_j$$

in Cartesian coordinates takes the form

$$\mathring{\mathbf{T}} \equiv \mathbf{T}(\tilde{\boldsymbol{V}} + \mathring{\boldsymbol{V}}) - \mathbf{T}(\tilde{\boldsymbol{V}}) = \begin{bmatrix} 0 & 0 & \mathring{V}_x \\ 0 & 0 & \mathring{V}_y \\ \mathring{V}_x & \mathring{V}_y & \mathring{V}_z \end{bmatrix} + \mathrm{O}(\mathring{V}^2). \tag{30}$$

The disturbance of the diffusive-dispersive salt flux (19), evaluated up to second-order terms, is:

$$\begin{aligned} \mathring{\boldsymbol{J}} &\simeq -(1 + \alpha_T \mathrm{Pe})\nabla\mathring{\omega} - \alpha_T \mathring{V}_z \nabla\tilde{\omega} - (\alpha_L - \alpha_T)(\mathring{\mathbf{T}}\nabla\tilde{\omega} + \mathbf{T}(\tilde{\boldsymbol{V}})\nabla\mathring{\omega}) \\ &= -(1 + \alpha_T \mathrm{Pe})\nabla\mathring{\omega} - (\alpha_L - \alpha_T)\frac{\mathrm{d}\tilde{\omega}}{\mathrm{d}z}\mathring{\boldsymbol{V}} \\ &\quad - \left[\alpha_T \frac{\mathrm{d}\tilde{\omega}}{\mathrm{d}z}\mathring{V}_z + \mathrm{Pe}(\alpha_L - \alpha_T)\partial_z\mathring{\omega}\right]\mathbf{e}_z. \end{aligned}$$

From (16), it follows that $\nabla\cdot\mathring{\boldsymbol{V}} = 0$. Hence,

$$\begin{aligned} -\nabla\cdot\mathring{\boldsymbol{J}} &= (1 + \alpha_T \mathrm{Pe})\nabla^2\mathring{\omega} + (\alpha_L - \alpha_T)\mathrm{Pe}\partial_{zz}^2\mathring{\omega} \\ &\quad + \alpha_T \frac{\mathrm{d}\tilde{\omega}}{\mathrm{d}z}\partial_z\mathring{V}_z + \alpha_L \frac{\mathrm{d}^2\tilde{\omega}}{\mathrm{d}z^2}\mathring{V}_z. \end{aligned} \tag{31}$$

Upon substituting (29), (31) into (16)–(19), we obtain the following set of equations for the disturbance quantities $\mathring{p}$, $\mathring{V}$ and $\mathring{\omega}$:

$$\nabla\cdot\mathring{V} = 0, \tag{32}$$

$$\partial_t\mathring{\omega} = (1+\alpha_T\mathrm{Pe})\nabla^2\mathring{\omega} + (\alpha_L-\alpha_T)\mathrm{Pe}\partial^2_{zz}\mathring{\omega} - \mathrm{Pe}\partial_z\mathring{\omega} +$$

$$+\alpha_T\frac{\mathrm{d}\tilde{\omega}}{\mathrm{d}z}\partial_z\mathring{V}_z - \left(\frac{\mathrm{d}\tilde{\omega}}{\mathrm{d}z} - \alpha_L\frac{\mathrm{d}^2\tilde{\omega}}{\mathrm{d}z^2}\right)\mathring{V}_z, \tag{33}$$

$$(1+\gamma\tilde{\omega})\mathring{V} = -\nabla\mathring{p} - (\mathrm{Ra}+\gamma\mathrm{Pe})\mathring{\omega}\mathbf{e}_z. \tag{34}$$

The boundary conditions for the disturbances at the bottom of the domain, take the form

$$z=0: \quad \mathring{p}=0, \quad \mathring{\omega}=0. \tag{35}$$

The boundary conditions at the top of the domain are more intricate. In the cases C1, C3, the entire top boundary is of $\mathcal{B}_1$-type, i.e., $\tilde{\omega}|_{z=1} < \omega_*$ and, hence, a slightly perturbed solution, $\omega = \tilde{\omega} + \mathring{\omega}$, should also satisfy $\omega < \omega_*$ at this boundary. The condition at the top of the layer is then

$$z=1: \quad \mathring{V}_z = 0, \quad \mathrm{Pe}\,\mathring{\omega} + \mathring{J}_z = 0 \quad (\tilde{\omega} < \omega_*). \tag{36}$$

In the case C2, the top boundary is of $\mathcal{B}_2$-type, i.e., $\tilde{\omega}|_{z=1} = \omega_*$, and the salt flux, $\mathrm{Pe}\,\tilde{\omega} + \tilde{J}_z$, is positive. If the perturbation of the salt flux, $\mathrm{Pe}\,\mathring{\omega} + \mathring{J}_z$, is small, then the disturbed salt flux is also positive, i.e., the disturbed solution also satisfies Dirichlet boundary condition at the top. For this case, we have

$$z=1: \quad \mathring{V}_z = 0, \quad \mathring{\omega} = 0, \quad (\mathrm{Pe}\,\tilde{\omega} + \tilde{J}_z > 0). \tag{37}$$

The set of Equations (32)–(34) may be reduced, by a standard procedure, to a single fourth-order equation with respect to $\mathring{V}_z$. However, in the future we intend to study a more realistic model of unsaturated flow (with saturation influenced by the flow), for which a reduction of this kind cannot be performed. For this reason, we shall just eliminate $\mathring{V}$ from (32)–(34), arriving at a set of two second-order equations for $\mathring{p}$ and $\mathring{\omega}$. We shall also make use of the fact that the transversal dispersivity is usually an order of magnitude less than the longitudinal one, and neglect the terms involving the factor α_T. Introducing the modified Rayleigh number, Ra', and the reduced concentration gradient, $F(z)$,

$$\mathrm{Ra}' = \mathrm{Ra} + \gamma\mathrm{Pe}, \quad F(z) = \frac{1}{\mathrm{Pe}'(1+\gamma\tilde{\omega})}\frac{\mathrm{d}\tilde{\omega}}{\mathrm{d}z},$$

and taking into account the exponential character of $\tilde{\omega}(z)$, we obtain:

$$\nabla^2\mathring{p} - \gamma\mathrm{Pe}'F(z)\partial_z\mathring{p} = \mathrm{Ra}'(\gamma\mathrm{Pe}'F(z)\mathring{\omega} - \partial_z\mathring{\omega}), \tag{38}$$

$$\partial_t \mathring{\omega} = \nabla^2 \mathring{\omega} + \alpha_L \mathrm{Pe}\, \partial_{zz}^2 \mathring{\omega} - \mathrm{Pe}\, \partial_z \mathring{\omega} + \\ + (1 - \alpha_L \mathrm{Pe}') F(z)(\partial_z \mathring{p} + \mathrm{Ra}' \mathring{\omega}). \tag{39}$$

Since these equations are linear, the variables can be separated. We shall seek solutions in the form

$$[\mathring{p}(\mathbf{x}, t),\ \mathring{\omega}(\mathbf{x}, t)] = [P(z), \Omega(z)]\, \mathrm{e}^{st + ilx + imy},$$

where the wavenumbers in the horizontal plane, l and m, are real, in order to keep the solution bounded as $x, y \to \pm\infty$. Substituting this into Equations (38)–(39), we obtain

$$(D^2 - \gamma \mathrm{Pe}' F D - a^2) P = \mathrm{Ra}'(\gamma \mathrm{Pe}' F - D)\Omega, \tag{40}$$

$$s\Omega = [(1 + \alpha_L \mathrm{Pe})D^2 - \mathrm{Pe}\, D - a^2]\Omega + \\ + \mathrm{Pe}'(1 - \alpha_L \mathrm{Pe}') F(DP + \mathrm{Ra}'\Omega), \tag{41}$$

where

$$D \equiv \frac{\mathrm{d}}{\mathrm{d}z}, \quad a = \sqrt{l^2 + m^2}.$$

The boundary conditions are

$$z = 0: \quad P = 0, \quad \Omega = 0, \tag{42}$$

$$z = 1: \quad DP + \mathrm{Ra}'\Omega = 0, \quad \begin{cases} \mathrm{Pe}'\Omega - D\Omega = 0 & \text{(case C2)} \\ \Omega = 0, & \text{(cases C1, C3).} \end{cases} \tag{43}$$

In these equations, the overall horizontal wavenumber, a, must be real (and, hence, a^2 must be nonnegative). The time exponent, s, may be complex, $s = \sigma + i\nu$. If the set (40)–(43) has a nonzero solution with $\sigma > 0$, the corresponding perturbation grows with time, i.e., we have instability. We are interested in the conditions of marginal stability, $\sigma = 0$. In general, at a marginal stability threshold, the frequency, ν, may differ from zero, i.e., the loss of stability may be by the oscillatory mode. For some close problems, however, it has been proven that $\nu = 0$ at the stability threshold — the so called *principle of exchange of stabilities* (see Nield [12], Homsy and Sherwood [7]). For this reason, we shall substitute $s = 0$ in (41). Note that although we cannot prove the exchange-of-stabilities principle for our problem, what we shall find is still *sufficient condition* for instability.

The homogeneous equations (40)–(43) form an eigenproblem in which any two of the three parameters, Ra', Pe', a^2, may be set arbitrary and the third regarded as

eigenvalue (there is also implicit dependence on Pe′ through the basic concentration gradient, $F(z)$). Homsy and Sherwood [7], in an analogous problem, fixed Pe′ and a^2, and solved for the lowest eigenvalue, $\mathrm{Ra}'(\mathrm{Pe}', a^2)$. Then, the linear stability limit is defined, in terms of nonmodified Rayleigh number, as

$$\mathrm{Ra}^*(\mathrm{Pe}') = \min_a \mathrm{Ra}'(\mathrm{Pe}', a^2) - \gamma \mathrm{Pe}\,.$$

For simplicity of calculations, it seems advantageous to invert the point of view and to regard a^2 as an eigenvalue, and Pe′ and Ra′ (or Ra) as parameters. This may be emphasized by transforming (40) and (41) (with $s = 0$) to the form

$$\mathcal{A}\begin{bmatrix} P \\ \Omega \end{bmatrix} = a^2 \begin{bmatrix} P \\ \Omega \end{bmatrix},$$

$$\mathcal{A} = \begin{bmatrix} (D - \gamma \mathrm{Pe}' F)D & \mathrm{Ra}'(D - \gamma \mathrm{Pe}' F) \\ \mathrm{Pe}'(1 - \alpha_L \mathrm{Pe}')FD & (D^2 - \mathrm{Pe}'D)/(1 - \alpha_L \mathrm{Pe}') \\ & + \mathrm{Ra}'\mathrm{Pe}'(1 - \alpha_L \mathrm{Pe}')F \end{bmatrix}. \tag{44}$$

The differential operator $\mathcal{A}$ is defined on the space of pairs of sufficiently smooth functions (P, Ω), satisfying the boundary conditions (42) and (43). If, for given Pe′ and Ra, the operator $\mathcal{A}(\mathrm{Pe}', \mathrm{Ra})$ has a *positive* eigenvalue a^2, then the basic solution is marginally stable. For a given Pe′, therefore, we are looking for the lowest Ra for which $\mathcal{A}(\mathrm{Pe}', \mathrm{Ra})$ has real positive eigenvalues. This lowest Rayleigh number is the linear stability limit, $\mathrm{Ra}^*(\mathrm{Pe}')$, corresponding to a given Pe′.

4.2. METHOD OF SOLUTION AND RESULTS

Following Jones and Persichetti [8], we solve the eigenproblem (44) numerically, using a second-order finite-difference scheme. However, the eigenfunctions of (44) corresponding to the positive a^2-eigenvalues prove to have an exponential character near $z = 1$. For this reason, the straightforward finite-difference approximation of (44) results in a very slowly converging procedure, especially for large Péclet numbers. To overcome this obstacle, we perform an exponential change of the independent variable, $z \to \zeta$, and normalize P and Ω to get rid of the large coefficients Ra′ and Pe′ in the boundary conditions

$$\zeta = \mathrm{e}^{\mathrm{Pe}'(z-1)}, \quad \overline{P} = P/\mathrm{Ra}', \quad \overline{\Omega} = \Omega/\mathrm{Pe}'. \tag{45}$$

Upon substituting (45) into (44) and dividing the first equation by $\mathrm{Ra}'(\mathrm{Pe}')^2$ and the second by $(\mathrm{Pe}')^3$, we obtain

$$\begin{bmatrix} \zeta^2 D^2 - \zeta(1 - \gamma F)D & (\zeta D - \gamma F) \\ \lambda \zeta F D & (1 + \alpha_L \mathrm{Pe})\zeta^2 D^2 - \lambda F \end{bmatrix} \begin{bmatrix} \overline{P} \\ \overline{\Omega} \end{bmatrix} = a^2 \begin{bmatrix} \overline{P} \\ \overline{\Omega} \end{bmatrix}, \tag{46}$$

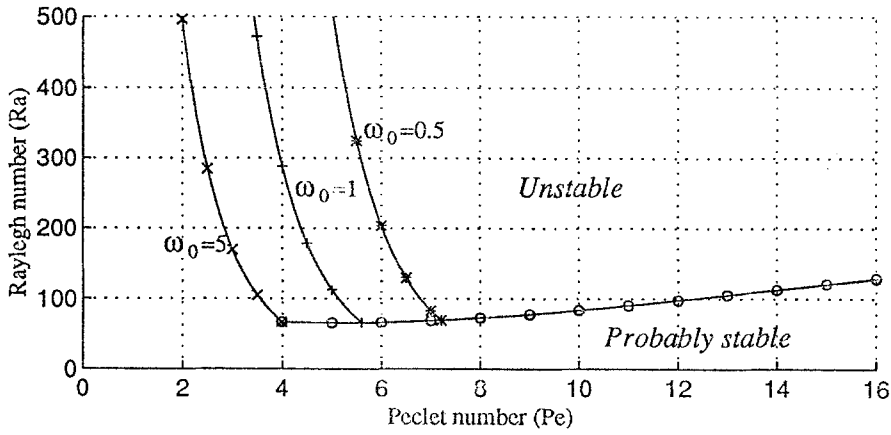

Figure 1. Linear stability limits $\mathrm{Ra}^*(\mathrm{Pe})$ ($\mathrm{Pe}' = \mathrm{Pe}$) of a 1-D vertical flow of saline water in porous layer with evaporation at the top. Mechanical dispersion is absent ($\alpha_L = 0$). The plots correspond to different initial concentrations, ω_0, given *pro mille*.

where D denotes now a derivative with respect to ζ, $\lambda = \mathrm{Ra}'/\mathrm{Pe}$, and a^2 is divided by $(\mathrm{Pe}')^2$. The boundary conditions transform into

$$\zeta = e^{-\mathrm{Pe}'} : \quad P = 0, \quad \Omega = 0, \tag{47}$$

$$\zeta = 1 : \quad D\overline{P} + \overline{\Omega} = 0, \quad \begin{cases} \overline{\Omega} - D\overline{\Omega} = 0 & (\tilde{\omega} < \omega_*) \\ \overline{\Omega} = 0, & (\mathrm{Pe}\,\tilde{\omega} + \tilde{J}_z > 0). \end{cases} \tag{48}$$

For the basic solutions C1–C3, the function $F(\zeta)$ has a form

$$F(\zeta) = \frac{\overline{\omega}\zeta}{1 + \gamma\overline{\omega}\zeta}, \quad \overline{\omega} = \begin{cases} \omega_0 \mathrm{e}^{\mathrm{Pe}'}, & \mathrm{Pe}' \le \mathrm{Pe}^* \\ \omega_*, & \mathrm{Pe}' \ge \mathrm{Pe}^*. \end{cases} \tag{49}$$

From (46)–(49), it is readily seen that for $\mathrm{Pe}^* > \mathrm{Pe}'$ the problem does not depend on concentration ω_0 at the bottom of the domain. For $\mathrm{Pe} \to \infty$, the only dependence on Pe preserved in the problem is through the factor $(1 + \alpha_L \mathrm{Pe})$ in the second equation (46).

In order to solve the eigenproblem, the differential operator on the left-hand side of (46) was replaced by its second-order finite-difference approximation, $\mathcal{A}_h$, taking the boundary conditions into account. The eigenvalues of $\mathcal{A}_h$ were calculated by using the standard function `eig()` of the MATLAB package. For a given Pe, the smallest value of λ for which the largest real eigenvalue of $\mathcal{A}_h$ is positive, was found by a binary search.

Grids of 20 to 120 nodes were tested to ensure the convergence of the method. The qualitative behavior of $\mathrm{Ra}^*(\mathrm{Pe}')$ was similar for all grids, including the coarsest. The scattering of the Ra^* values was generally less than 2% for grids with 50 nodes

and more; for a relatively small Pe (Pe′ far from $1/\alpha_L$), this scattering was less than 0.5%. The results are presented in Figures 1 and 2.

We examined two basic solutions for $\mathrm{Pe}' > \mathrm{Pe}^*$: C2, which corresponds to a steady state, and C3, which corresponds to a transient state, just before the onset of precipitation. It was found that C2 is always more stable with respect to small perturbations than C3. For this reason the results presented correspond to C1 for $\mathrm{Pe}' \leq \mathrm{Pe}^*$ and to C3 for $\mathrm{Pe}' > \mathrm{Pe}^*$.

In the first series of calculations, mechanical dispersion was neglected ($\alpha_L = 0$, and, hence, $\mathrm{Pe}' = \mathrm{Pe}$). The dependencies $\mathrm{Ra}^*(\mathrm{Pe})$ obtained for various values of groundwater salinity, ω_0, are presented in Figure 1. For the maximal solubility and for the viscosity variation coefficient the values $\omega_* = 0.27$ and $\gamma = 2.3$ were used, which correspond to the properties of NaCl solution.

Every curve in the Figure 1 divides the entire domain of possible Pe and Ra' values in two parts. The upper subdomain corresponds to instability of 1-D flow regime. In principle, because of the number of simplifications employed, nothing definite may be said about the lower subdomain. In addition to stable solutions, the latter may contain also solutions which are stable for small perturbations, but unstable for finite ones, as well as those which lose stability by nonmonotonic mode (so-called 'overstability').

As expected, the region of instability is convex, and Ra^* depends on Pe in a nonmonotonic way. This means that for large enough Ra', the 1-D solution is stable either when evaporation is extremely slow (when the salinity gradient is small) or when it is very intensive. In the intermediate Pe range instability is expected. As Pe increases, Ra^* decreases rapidly at first, reaching a minimal value at about $\mathrm{Pe} = \mathrm{Pe}^*(\omega_0) \equiv \ln(\omega_*/\omega_0)$. This is due to the simple physical reason that the increase in Pe causes an increase in the salinity gradient, $F(\zeta)$, which is the source of instability. As is readily seen from (49), for a fixed Pe, this gradient increases with ω_0. This fact explains the shift between the curves that correspond to different ω_0: the more saline is groundwater the more unstable is the 1-D steady flow.

When Pe exceeds Pe^*, the problem does not depend on ω_0, and, hence, all graphs have a common right branch. For large Pe, the boundary condition (47) may be moved to the point $\zeta = 0$. The problem (46)–(48) will depend then only on the ratio $\lambda = \mathrm{Ra}'/\mathrm{Pe}$. The minimal value of λ for which (46) has positive eigenvalues a^2 was found to be $\lambda^* = 10.3$ (for $\gamma = 2.3$). Thus, for large Pe, the instability threshold Ra^* has a linear asymptote, $\mathrm{Ra}^* = (\lambda^* - \gamma)\mathrm{Pe}$.

Even more important than the particular form of $\mathrm{Ra}(\mathrm{Pe})$ dependencies is the order of magnitude of the critical Rayleigh numbers. It can be seen that a Ra number of several hundreds is usually large enough to cause instability. On the other hand, we may estimate realistic Ra numbers for moisture movement in the unsaturated zone. Taking for the estimate $k = 2 \times 10^{-14}\mathrm{m}^2$, $\beta = 0.6$, $g = 10\mathrm{m/s}$, $H = 2\mathrm{m}$, $\mu_0/\rho_0 = 10^{-6}\mathrm{m}^2/\mathrm{s}$, $\theta\mathcal{D}^* = 0.3 \times 10^{-10}\mathrm{m}^2/\mathrm{s}$, we obtain

$$\mathrm{Ra} = \frac{k\beta g H}{(\mu_0/\rho_0)\theta\mathcal{D}^*} = 800.$$

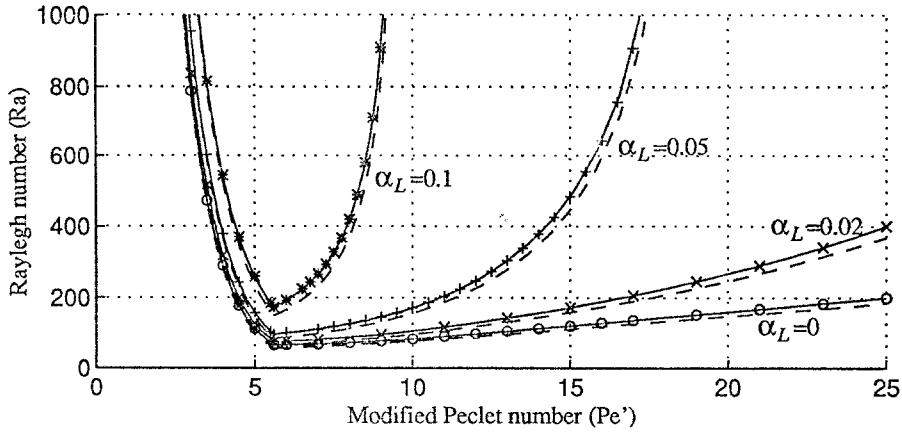

Figure 2. Influence of longitudinal dispersivity on the stability limits, $\mathrm{Ra}^*(\mathrm{Pe}')$. The plots correspond to different values of the dimensionless dispersivity, α_L. Solid lines: $\gamma = 2.3$, dashed lines: $\gamma = 0$.

Thus, instability is very likely in real situations.

In Figure 2, the graphs corresponding to different values of dimensionless diffusivity, α_L, are shown in the $(\mathrm{Ra}', \mathrm{Pe}')$- plane. Each curve (except for that corresponding to $\alpha_L = 0$) has a vertical asymptote at $\mathrm{Pe}^* = 1/\alpha_L$.

Solid lines correspond to the viscosity variation coefficient $\gamma = 2.3$, while dashed lines correspond to the case when viscosity is independent on concentration ($\gamma = 0$). The influence of viscosity variations is twofold. On one hand, the intrusion of fresher, less viscous water in the overlaying layer filled with saline, more viscous water may cause Saffman–Taylor instability. This effect is represented by the term $\gamma \mathrm{Pe}$ on the r.h.s. of (34). On the other hand, the greater is γ the larger is the viscous resistance to the velocity perturbations. The latter effect, which is represented by the factor of $(1 + \gamma\tilde{\omega})$ on the l.h.s. of (34), is neglected in most studies, because the variation of the basic concentration itself is, usually, small. However, this is not the case here. It can be seen from Figure 2 that the two mentioned effects almost neutralize each other, with the second being even stronger (larger γ correspond to slightly more stable solutions).

The fact that the basic concentration gradient is not small has one additional interesting consequence. The coefficient of hydrodynamic dispersion for the uniform basic flow, if the transversal diffusivity is neglected, is expressed as

$$\mathbf{D}_h = \begin{bmatrix} 1 & 0 & 0 \\ 0 & 1 & 0 \\ 0 & 0 & 1 + \alpha_L \mathrm{Pe} \end{bmatrix} \mathcal{D}^*, \tag{50}$$

where $\mathcal{D}^*$ is the diffusion coefficient. We may consider the tensor (50) as some anisotropic 'enhanced' diffusion coefficient. At first glance, as long as only small velocity perturbations are studied, we might expect that the influence of mechan-

ical dispersion on stability is confined to such 'enhancement' of the diffusion coefficient. However, this is not the case, and the replacement of dispersion by the 'enhanced' diffusion results in a different asymptotics for the critical Rayleigh number at large Pe. Actually, the case of 'enhanced' diffusion may be reduced to the same eigenproblem (46), but with λ denoting $\mathrm{Ra}'/\mathrm{Pe}'$ instead of Ra'/Pe as before. Thus,

$$\mathrm{Ra}^*_{DF} = (1 + \alpha_L \mathrm{Pe})^{-1} \mathrm{Ra}^*,$$

where Ra^*_{DF} corresponds to the 'enhanced' diffusion.

5. Simulation of Convective Flows

We have shown that the one-dimensional vertical flow is usually unstable and, therefore, the real flow has a two- or three-dimensional structure (and may even be unsteady). This fact makes it necessary to use a numerical simulation to study the flow pattern at high Rayleigh numbers and the influence of free convection on the distribution of salt in the unsaturated zone.

We shall seek, numerically, two-dimensional steady solutions of (16)–(22). We shall use the multigrid approach which was successfully applied to the simulation of thermally induced convection in a pure liquid (e.g., Thompson *et al.* [14], Wesseling [15]) as well as in a porous medium (Dawood and Burns [5]). For this purpose, we shall discretize the steady-state equations using the Finite Volume Element Method due to McCormick [10], arriving at a set of nonlinear algebraic equations, and then solve them by the Full Approximation Storage Algorithm [13].

5.1. PROBLEM FORMULATION FOR THE NUMERICAL SOLUTION

We seek steady state solutions of (16)–(22) in the xz-plane. Because the field of flow rate is solenoidal, the stream function, $\psi(x, z)$, can be defined:

$$\boldsymbol{V} = \begin{bmatrix} V_x \\ V_z \end{bmatrix} = \begin{bmatrix} \partial_z \psi \\ -\partial_x \psi \end{bmatrix}. \tag{51}$$

It is convenient to choose the stream function and the concentration as the primary variables. Then (16) is automatically satisfied, and from (18) we obtain

$$\nabla \cdot (1 + \gamma\omega) \nabla\psi - \mathrm{Ra}\, \partial_x \omega = 0. \tag{52}$$

The steady-state salt balance equation takes the form

$$\nabla \cdot (\boldsymbol{V}\omega - \mathbf{D}_h \omega) = 0, \tag{53}$$

where the coefficient of hydrodynamic dispersion is a symmetrical second rank tensor, which is expressed in the (x, z) coordinates as

$$\mathbf{D}_h = (1 + \alpha_L V)\mathbf{I} + \frac{\alpha_L - \alpha_T}{V} \begin{bmatrix} V_x^2 & V_x V_z \\ V_x V_z & V_z^2 \end{bmatrix}. \tag{54}$$

We shall seek a solution to (51)–(53) in the rectangular domain

$$0 < x < L, \quad 0 < z < 1. \tag{55}$$

Along the lateral sides of this rectangle we shall use a no-flux boundary condition. Thus, the full set of boundary conditions takes the form:

$$x = 0 : \qquad \psi = 0, \quad (\mathbf{D}_h \nabla \omega) \cdot \mathbf{e}_x = 0, \tag{56}$$

$$x = L : \quad \psi = -\mathrm{Pe}\, L, \ (\mathbf{D}_h \nabla \omega) \cdot \mathbf{e}_x = 0, \tag{57}$$

$$z = 0 : \qquad \partial_z \psi = 0, \quad \omega = \omega_0, \tag{58}$$

$$z = 1 : \quad \psi = -\mathrm{Pe}\, x, \ \begin{cases} \mathrm{Pe}\,\omega - (\mathbf{D}_h \nabla \omega) \cdot \mathbf{e}_z = 0, & (\omega \le \omega_*), \\ \omega = \omega_*, & (\mathrm{Pe}\,\omega - (\mathbf{D}_h \nabla \omega) \cdot \mathbf{e}_z \ge 0). \end{cases} \tag{59}$$

As explained earlier, with respect to ω, it is a Dirichlet condition along some (unknown!) part of the boundary ($\mathcal{B}_2$) and a Cauchy one along the remaining part ($\mathcal{B}_1$). In the current work we shall address only the case when the Cauchy condition prevails along the entire boundary. This assumption may be verified a-posteriori.

5.2. DISCRETIZATION

We have chosen the *Finite Volume Elements Method* (FVEM) for discretization of the problem. This is a combination of the method of finite volumes, which is widely used for constructing conservative and physically reasonable finite difference schemes in a variety of transport problems, with the ideology of the finite-element approach.

Let a set of partial differential balance equations be defined in some region Ω. The methodology of FVEM (see [10]) involves the following steps:

(1) A grid $G = \{\mathbf{x}_m, \ m = 1, \ldots, N\}$ in Ω is defined and some *control volume*, $\mathcal{U}_m$, is associated with every grid node, $\mathbf{x}_m$. The control volumes are chosen in such a way as to provide a partitioning of Ω.

(2) Balance equations are written for each $\mathcal{U}_m$ in an integral form (i.e., the increase of certain extensive quantity in $\mathcal{U}_m$ equals to its internal production minus the net outflux through the boundary of $\mathcal{U}_m$).

(3) The unknowns are replaced by their finite-element approximations, e.g., by the linear combination of their nodal values multiplied by appropriate 'hat functions'. The fluxes, production terms, etc., are then expressed, using these approximations, in terms of the nodal values of the unknowns, resulting in a set of algebraic equations.

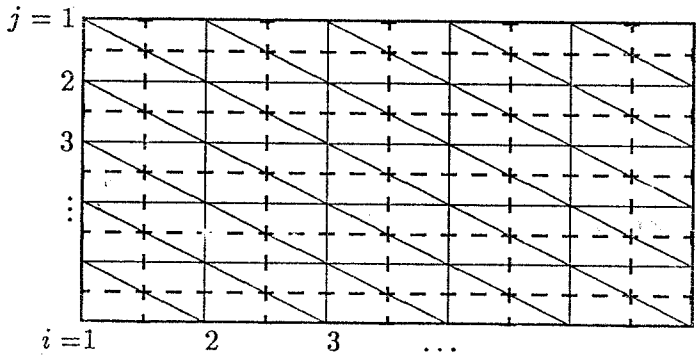

Figure 3. Finite element triangulation (solid lines) and control volumes (dashed lines).

The FVEM may be considered as a particular case of the Petrov–Galerkin method, in which indicator functions of control volumes are used as weight functions. The FVEM seems a very attractive choice, because it preserves the close connection with the physical sense of the problem, which is a strong feature of the method of finite volumes, with the universal and systematic character of the finite elements approach, which has a strong theoretical basis.

For simplicity, we use linear finite elements with the triangulation shown in Figure 3. In every individual triangle, ω and ψ are approximated by linear functions*. The control volume partitioning of the region is shown in the same figure in dashed lines. All control volumes, except for those attached to the boundary, are $\Delta x \times \Delta z$-rectangles centered at nodal points. An individual node and the control volume associated with it are specified by the pair (i, j) as shown.

For each control volume, $\mathcal{U}_{ij}$, integral analogues of (52) and (53) (i.e., vorticity balance and salt mass balance in the control volume) may be written. Replacing 2-D integrals by contour ones, using the divergence theorem, we obtain:

$$\int_{S_{ij}} [(1 + \gamma\omega)\nabla\psi - \mathrm{Ra}\,\omega\mathbf{e}_x] \cdot \boldsymbol{n}\,\mathrm{d}s = 0, \tag{60}$$

$$\int_{S_{ij}} \left[\omega(s)\frac{\mathrm{d}\psi}{\mathrm{d}s} - \mathbf{D}_h\nabla\omega \cdot \boldsymbol{n}\right] \mathrm{d}s = 0, \tag{61}$$

where S_{ij} is the boundary of $\mathcal{U}_{ij}$. Within every triangle, ψ and ω are replaced by their linear approximations. The integrals are then calculated in a straightforward manner, and expressed through the nodal values, ω_i^j and ψ_i^j, which serve as unknowns in the discretized equations.

* More intricate approximation making use of exponential shape functions may be necessary in the case of large advective fluxes (i.e., large Pe and/or Ra numbers) to prevent numerical instability when the problem is solved on a coarse grid. Such approximation is the FVEM analog of upwind approximation (see McCormick [10]).

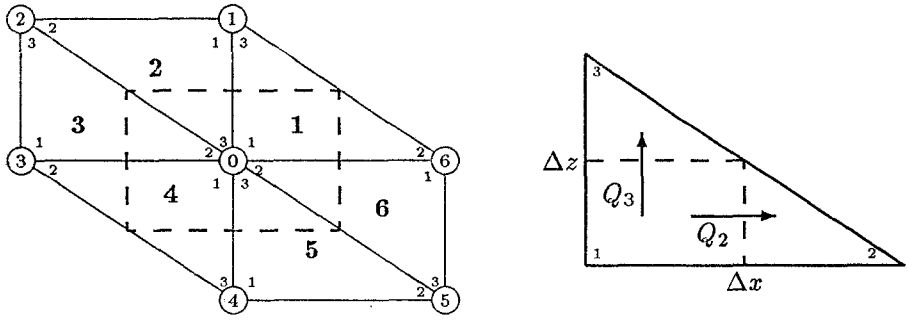

Figure 4. Local numbering associated with a control volume (dashed rectangle). Local node numbers are in the circles, local numbers of elements are in bold. Small numbers near the nodes denote their *intraelement* numbers.

The obtained system inherits the quasilinear character of (60)–(61), i.e., the discrete analogue of (60) is linear with respect to ψ_i^j, while the discrete analogue of (61) is linear with respect to ω_i^j. Since we are going to solve the system by using multigrid iterative method, we do not need to hold the entire matrix of the system except for the coarsest grid. For this reason, it is convenient to introduce the *local numbering* of nodes and elements associated with each control volume, as shown in the Figure 4. Any control volume (except for those adjacent to the borders) intersects with six triangle elements which, in total, have seven different nodes. The discrete analogues of (60)–(61) may be written, using the local numbering, as follows:

$$Q^{(\psi)} \equiv \sum_{l=0}^{6} a_l \psi_l + f = 0, \quad Q^{(\omega)} \equiv \sum_{l=0}^{6} b_l \omega_l + g = 0, \tag{62}$$

where l is the local node number, the coefficients a_l and f depend on ω_k, $k = 0, \ldots 6$, while b_l depends on ψ_k, $k = 0, \ldots 6$.

Following the finite element methodology, we 'assemble' the vectors of coefficients, $\{a_0, \ldots, a_6, f\}$ and $\{b_0, \ldots, b_6, g\}$, by summing up the contributions of the individual elements into the total vorticity ($Q^{(\psi)}$) and salt ($Q^{(\omega)}$) fluxes through the boundary of the control volume. Each element can be mapped linearly into the standard one presented in Figure 4. Thus, all flux calculations should be performed only for the standard element.

Introducing the *intraelement* numbering of nodes ($m = 1, \ldots 3$), and using linear approximations of ψ and ω in the element, we obtain the following expressions for the vorticity fluxes, $Q_m^{(\psi)}$, towards the node m:

$$Q_1^{(\psi)} = -(Q_2^{(\psi)} + Q_3^{(\psi)}),$$

$$Q_2^{(\psi)} = 0.5a(1 + \gamma\overline{\omega}_2)(\psi_2 - \psi_1) \pm 0.5\Delta z \mathrm{Ra}\,\overline{\omega}_2,$$

$$Q_3^{(\psi)} = 0.5a^{-1}(1 + \gamma\overline{\omega}_3)(\psi_3 - \psi_1),$$

where $\overline{\omega}_2, \overline{\omega}_3$ are the mean concentrations along the corresponding midlines,

$$\overline{\omega}_2 = \frac{\omega_1 + 2\omega_2 + \omega_3}{4}, \quad \overline{\omega}_3 = \frac{\omega_1 + 2\omega_3 + \omega_2}{4},$$

and $a = \Delta z/\Delta x$ is the aspect ratio of the element. The sign in the expression for $Q_2^{(\psi)}$ depends on whether the mapping of the element into the standard one is a central symmetry (+), or just a translation (−). Similarly, mass fluxes of salt are expressed as follows:

$$\begin{aligned}
Q_1^{(\omega)} &= -(Q_2^{(\omega)} + Q_3^{(\omega)}), \\
Q_2^{(\omega)} &= \frac{V_x \Delta z}{8}\overline{\omega}_2 - \frac{a}{2}\left(1 + \alpha_L \frac{V_x^2}{V} + \alpha_T \frac{V_z^2}{V}\right)(\omega_2 - \omega_1) \\
&\quad -(\alpha_L - \alpha_T)\frac{V_x V_z}{2V}(\omega_3 - \omega_1), \\
Q_3^{(\omega)} &= -\frac{V_z \Delta x}{8}\overline{\omega}_3 - \frac{1}{2a}\left(1 + \alpha_T \frac{V_x^2}{V} + \alpha_L \frac{V_z^2}{V}\right)(\omega_3 - \omega_1) \\
&\quad -(\alpha_L - \alpha_T)\frac{V_x V_z}{2V}(\omega_2 - \omega_1),
\end{aligned}$$

where

$$V_x = \frac{\psi_3 - \psi_1}{\Delta z}, \quad V_z = -\frac{\psi_2 - \psi_1}{\Delta x}.$$

5.3. FAS ALGORITHM

We have to solve the set of quasilinear algebraic equations (62) defined on the grid G. The basic multigrid technique used for this purpose is the Full Approximation Storage (FAS) method (see [13], [3]).

The FAS algorithm can be briefly described as follows. Let a sequence of increasingly finer grids, G^k, $k = 1, 2 \ldots K$, be given. (In practice, we choose the spacing $[\Delta x_k, \Delta z_k]$ of G^k to be half of $[\Delta x_{k-1}, \Delta z_{k-1}]$.) Let U^k be the set of grid vector-functions $G^k \to \mathbf{R}^m$ on G^k, where m is the number of scalar differential equations being solved. Let there be given two transfer operators: *prolongation*, $\mathcal{P}^k : U^{k-1} \to U^k$, and *restriction** , $\mathcal{R}^k : U^k \to U^{k-1}$.

* Two different restriction operators may be used: one for the transfer of the residues and the other for the solution.

The problem to be solved is then represented by the form:

$$\mathcal{L}^k(u^k) = f^k, \quad u^k, f^k \in U^k, \tag{63}$$

where the (nonlinear) operator $\mathcal{L}^k : U^k \to U^k$ is the discretization of the differential operator of interest on the grid G^k. Although $f^1 = 0$ on the finest grid, nonzero right-hand side arises on the other grids in the course of 'coarsening'.

On every grid, a smoothing operator should be defined, $\mathcal{S}^k : U^k \times U^k \times \mathbf{N} \to U^k$. The smoothing procedure is assumed to suppress high-frequency components of the error. We denote the result of ν smoothing iterations applied to the initial guess u^k by $\mathcal{S}^k(u^k, f^k, \nu)$.

The FAS multigrid correction operator, $\mathcal{F}^k(u^k, f^k, \mu, \nu)$, returns an improved approximation of the solution of (63), given an initial approximation u^k. The parameters μ and ν denote the number of post- and pre-smoothing iterations respectively. The multigrid correction operator $\mathcal{F}^k : U^k \times U^k \times \mathbf{N}^2 \to U^k$, can be defined recursively. On the coarsest grid ($k = 1$), $\mathcal{F}^1$ should solve (63) by any direct or iterative method. On any finer grid $\mathcal{F}^k$ is defined through $\mathcal{F}^{k-1}$ by the following steps.

1° *Pre-smoothing:* $u^k_{(1)} = \mathcal{S}^k(u^k, f^k, \nu), \quad r^k = f^k - \mathcal{L}^k(u^k_{(1)})$;

2° *Coarsening:* $u^{k-1} = \mathcal{R}^k u^k_{(1)}, \quad f^{k-1} = \mathcal{L}^{k-1}(u^{k-1}) + \mathcal{R}^k r^k$;

3° *Coarse-grid solution** : $\tilde{u}^{k-1} = \mathcal{F}^{k-1}(u^{k-1}, f^{k-1})$;

4° *Coarse-grid correction:* $u^k_{(2)} = u^k_{(1)} + \mathcal{P}^k(\tilde{u}^{k-1} - u^{k-1})$;

5° *Post-smoothing:* $u^k_{(3)} = S^k(u^k_{(2)}, f^k, \mu)$.

By definition,

$$\mathcal{F}^k(u^k, f^k, \mu, \nu) = u^k_{(3)}.$$

The above algorithm was implemented in the program CONVEX written in C language. The `mgfas()` function from the *Numerical Recipes C library* [13] was used as a prototype. We used bilinear interpolation for the prolongation and full weighting for the restriction operator. The smoothing was performed by nonlinear red-black Gauss–Seidel relaxation.

On the coarsest grid, Picard iterations were used to get rid of the nonlinearity. At every step, the discrete analogue of (53) was solved by direct method with respect to ω, taking ψ as found in the previous iteration. Then the discrete analogue of (52) was solved with respect to ψ, using the distribution of ω just found.

* By this definition of coarse grid solution, we choose the so called 'V-cycles'. Two iterations of $\mathcal{F}^{k-1}$ would lead to 'W-cycles', etc.

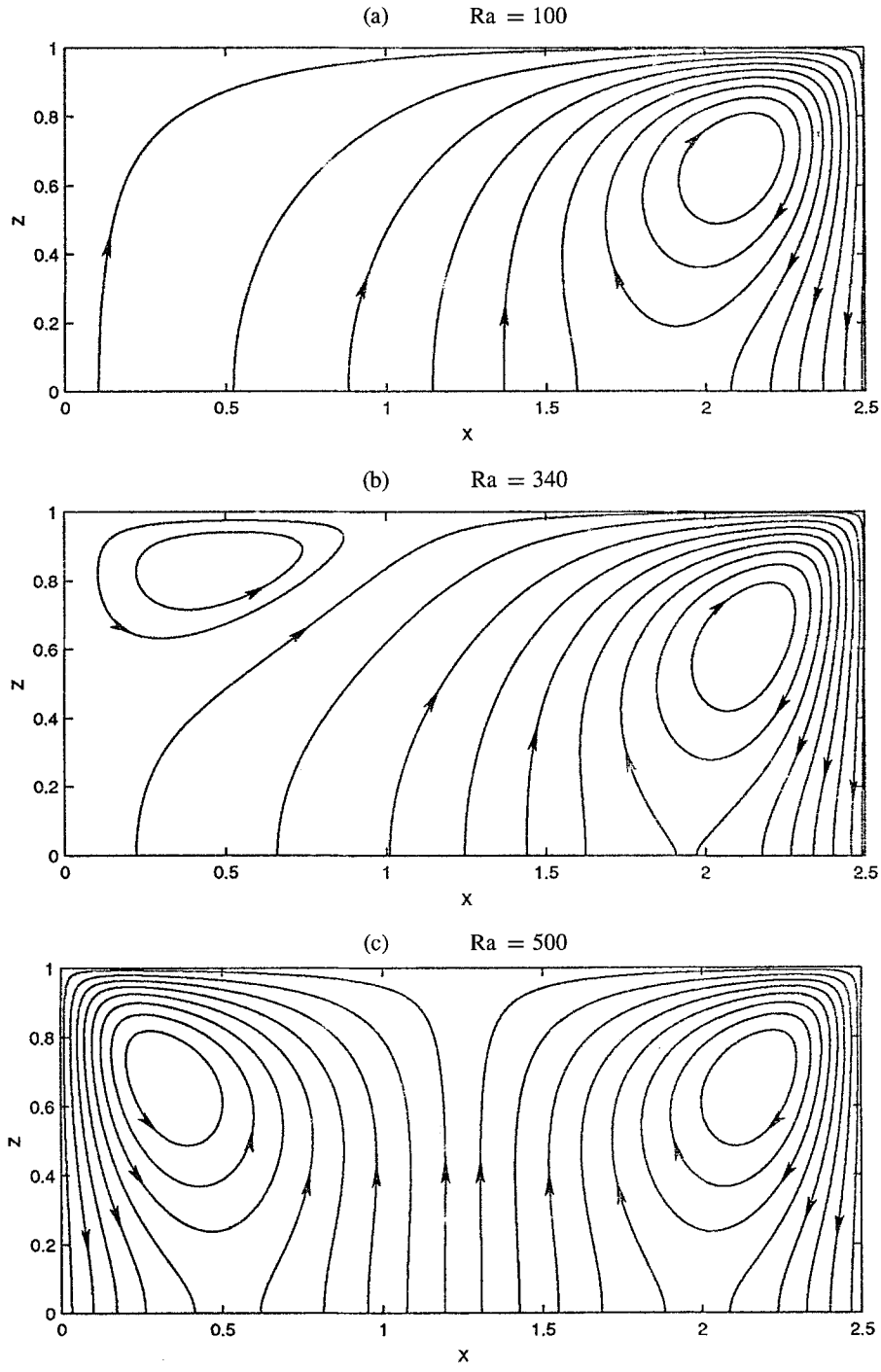

Figure 5. Evolution of the flow structure with Ra. Streamlines of *net* convective currents, $\mathring{\psi} = \psi + \mathrm{Pe}\, x$, are shown for $\mathrm{Pe} = 6$, $\gamma = 2.3$, $L = 2.5$, $\omega_0 = 1‰$. At $\mathrm{Ra} \simeq 340$ single convective cell divides into two.

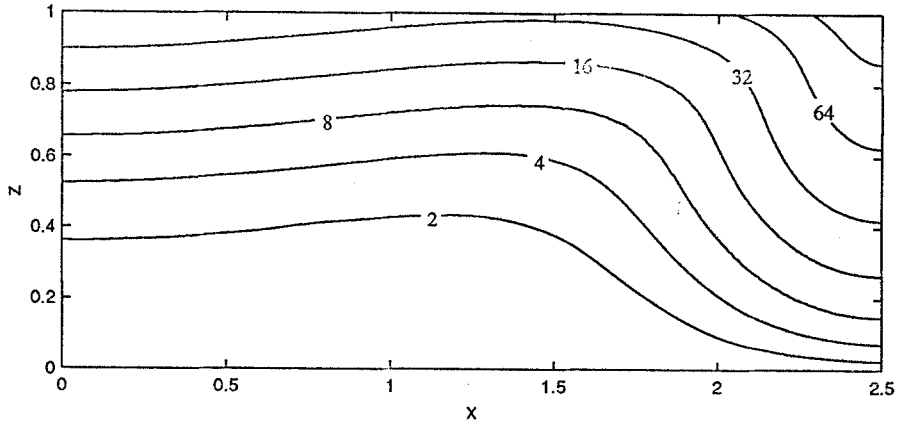

Figure 6. Steady-state distribution of concentration (values of ω are given *pro mille*). Pe $= 6$, Ra $= 340$, $\gamma = 2.3$, $L = 2.5$, $\omega_0 = 1‰$.

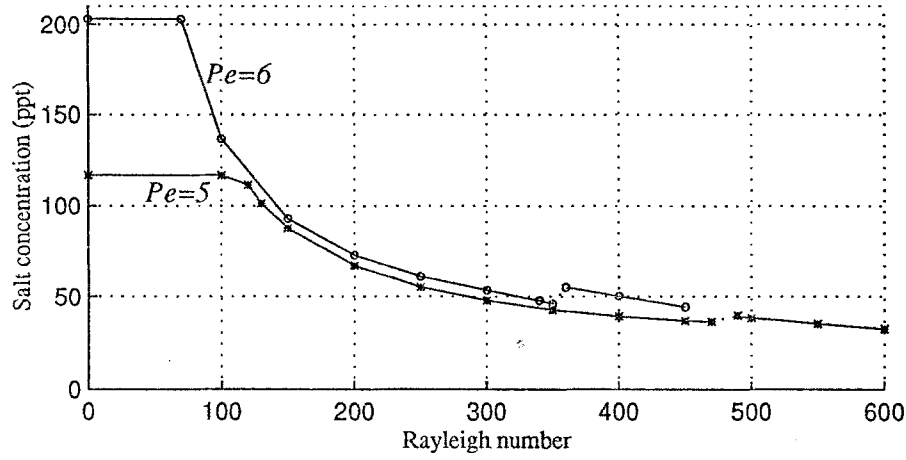

Figure 7. Dependence of the average salt concentration near ground surface on the Ra number. $L = 2.5$, $\omega_0 = 1‰$.

5.4. RESULTS OF 2-D SIMULATION

Grids up to 1000×250 were used in the simulation runs. The algorithm demonstrated a very fast convergence for relatively low Rayleigh numbers, but failed to converge for large Ra (the threshold depends primarily on Pe and ω_0). This is, apparently, because of the failure of Picard iterations on the coarsest grid. All simulation results address the case without mechanical dispersion ($\alpha_L = \alpha_T = 0$).

In Figure 5 the typical evolution of the flow structure with the increase of Ra is presented. In this figure the streamlines of *net* convective current are shown, i.e., the levels of the *net* stream function, $\mathring{\psi} = \psi - \tilde{\psi}$, where $\tilde{\psi} = -\mathrm{Pe}\, x$ is the stream

function of 1-D vertical flow. Note, that the ground surface is impermeable for the net convective currents.

The convective cells width is influenced, of course, by the width of the entire region, L. Trying very wide regions, we have determined an approximate width of the convective cells for some conditions (Pe $= 6$, Ra $= 100, \omega_0 = 1‰$) and then set L to this width for successive runs with larger Ra numbers. It should be noted that the flow in a cell is not symmetric: upward stream is slow, but wide, while the downward stream is fast and narrow. The increase of Rayleigh number causes a reduction in the width of the convective cells. The development of a new cell in the stagnation zone is shown in Figure 5(b).

The 2-D steady-state distribution of salt in the vertical plane, corresponding to the flow pattern of Figure 5(b), is shown in Figure 6. It can be seen that the local salt concentration is reduced significantly (two to ten times) compared with the 1-D distribution (24).

In Figure 7, the averaged concentration of salt near ground surface (the upper 10% of the soil layer were taken) is plotted versus the Rayleigh number. The results are presented for $\omega_0 = 1‰$ and two Péclet numbers: Pe $= 6$ (the upper curve) and Pe $= 5$ (the lower curve). It should be noted, that though for 1-D solutions the concentrations near the ground surface differ sharply (almost twice), after the onset of convection the difference between the two cases is minor. The surface concentration decreases, approximately, as Ra^{-1}. The nonmonotonicity of the curves is related to the change in the flow regime: splitting of a convection cell in two narrower ones. Probably, this nonmonotonicity can be addressed to influence of the finite width of the simulated region.

6. Conclusions

We have studied steady (or quasi-steady) flow of saline water in the vadoze zone, caused by evaporation from ground surface. We used a simplified mathematical model which takes into account hydrodynamic dispersion and the influence of salt concentration on viscosity.

By means of a linear perturbation analysis, we have studied the conditions under which the uniform vertical flow becomes unstable. The arising eigenvalue problem was solved numerically by the method of finite differences. The stability limit (critical Rayleigh number separating linearly stable and unstable regimes) was determined as a function of the Péclet number for various concentrations of salt in groundwater and for various porous medium dispersivities. It was shown that the loss of stability corresponds to quite realistic Rayleigh numbers. The stability limit depends in a nonmonotonic way on the evaporation rate. Viscosity variations with changing salt concentration, though much larger than those of density, were shown to have a minor influence on the stability.

A 2-D numerical model was used to study the flow pattern and salinity profile in the developed convective regime. Finite Volume Element discretization was used in

conjunction with FAS multigrid algorithm resulting in a highly effective procedure. It was found that mean salt concentration in the upper soil layer decreases with Rayleigh number (approximately, as Ra^{-1}) and that this concentration is much less sensitive to the evaporation rate than in the case when free convection is excluded.

Acknowledgement

The second author wishes to acknowledge the support of the Fund for the Promotion of Research at the Technion for partial support of this research.

References

1. Bear, J. and Bachmat, Y.: *Introduction to Modelling of Transport Phenomena in Porous Media*, Kluwer Acad. Publ., Dordrecht, 1990.
2. Bear, J. and Gilman, A.: Migration of salts in the unsaturated zone caused by heating, *Transport in Porous Media* **19**(2) (1995), 139–156.
3. Brandt, A.: *Multigrid Techniques: 1984 Guide with Applications to Fluid Dynamics, Computational Fluid Dynamics*, von Karman Inst, Belgium, 1984.
4. Bresler, E., McNeal, B. L., and Carter, D. L.: *Saline and Sodic Soils*. Springer-Verlag, New York, 1982.
5. Dawood, A. S. and Burns, P. J.: Steady three-dimensional convective heat transfer in a porous box via multigrid. *Int. J. Heat Mass Transfer* **22** (1992), 167–198.
6. Hillel, D.: *Applications of Soil Physics*. Academic Press, New York, 1980.
7. Homsy, G. M. and Sherwood, A. E.: Convective instabilities in porous media with through flow, *AIChE* **22**(1) (1976), 168–174.
8. Jones, M. C. and Persichetti, J. M.: Convective instabilitiy in packed beds with throughflow. *AIChE*, **32**(9) (1986), 1555–1557.
9. Joseph, D. D.: *Stability of Fluid Motions*, volume 2, Springer-Verlag, New York, 1976.
10. McCormick, S. F.: *Multilevel Adaptive Methods for Partial Differential Equations*. Frontiers in Applied Math., SIAM, Philadelphia, 1989.
11. Monteith, J. L.: The development and extension of Penman's evaporation formula, in. *Applications of Soil Physics* [6], pp. 247–253.
12. Nield, D. A. and Bejan, A.: *Convection in Porous Media*, Springer-Verlag, New York, 1992.
13. Press, W. H., Teukolsky, S. A., Vetterling, W. T., and Flannery, B. P.: *Numerical Recipes in C: The Art of Scientific Computing*, Cambridge University Press, 1992.
14. Thompson, C. P., Leaf, G. K., and Vanka, S. P.: Application of a multigrid method to a buoyancy-induced flow problem. in S. F. McCormick, (ed), *Multigrid Methods*, 1988, pp. 605–629.
15. Wesseling, P.: *An Introduction to Multigrid Methods*. Wiley, New York, 1992.
16. Wooding, R. A.: Rayleigh instability of a thermal boundary layer in flow through a porous medium. *J. Fluid Mech.* **9** (1960), 183–192.